From: **Conjugated Polymer and Molecular Interfaces**, Chapter 11, Salaneck, Seki, Kahn, and Pireaux (editors), Marcel Dekker, 2002.

# Organic Molecular Interfaces: Investigations of Electronic Structure, Chemistry and Carrier Injection Properties

*C. Shen and A. Kahn*

Department of Electrical Engineering, Princeton University, Princeton, NJ 08544, USA

and

*I.G. Hill*

Sarnoff Corporation, Princeton, NJ 08543, USA

## I. Introduction

The contributions included in this book underscore the importance of the structural, chemical and electronic properties of interfaces in organic devices. The progress made in the past decade in developing new multi-color organic light emitting diodes (OLEDs) [1-7], optically and electrically pumped lasers [8,9], thin film transistors [10-13] and solar cells [14,15] is pulling the field of organic polymers and small molecule materials at an astounding pace. The vast majority of these devices have a thin film architecture, which comprises multiple organic-inorganic and organic-organic interfaces [1-7]. Because of the very nature of thin film devices, these interfaces are generally located within a few molecular planes from active regions. Their electronic and chemical properties determine the characteristics of charge carrier injection into and transport through the device. OLEDs require that injection of electrons and holes be balanced in order to maximize device quantum efficiency (Fig. 1). The injection of these charge carriers must be efficient and stable under operation. Metal/organic contacts undergo complex and spatially extended chemical interactions, which can dominate the electrical properties of interfaces. Organic/organic heterojunctions in OLEDs control the transport of carriers between layers and the region of the device where recombination takes place. Understanding the mechanisms that control the interface electronic structure, including the impact of interface chemistry on carrier injection, is therefore of paramount importance for a more directed engineering of organic devices.

Considerable progress is being made in the area of device efficiency and reliability, although much of it has so far been achieved by empirical means. The drive to develop technologically viable and marketable devices has often left behind the science required to fully understand the mechanisms at play. Over the past decade, however, surface science has begun to play a key role in developing a deeper fundamental understanding of organic interfaces [16], particularly with respect to the way electronic structure and chemistry relate to charge carrier injection. As a consequence, the level of theoretical and experimental understanding of organic interfaces has improved to the point where some predictability is possible. This understanding is still limited, however, in comparison to what has been achieved for interfaces of inorganic semiconductors.

The molecular nature of organic films makes the investigation of their interface properties both experimentally more flexible and theoretically more challenging than for inorganic semiconductors. The flexibility derives from the fact that organic molecular films with good electronic and optical properties can be formed on a variety of substrates under a broad range of deposition conditions. Inorganic semiconductors must be grown epitaxially or must be passivated to reduce the density of electronically active defects associated with unsaturated covalent bonds (e.g. hydrogenated amorphous silicon). Lattice matching and temperature compatibility put strict constraints on the choice of substrate and growth conditions for epitaxial layers. Organic molecular films, on the other hand, are not bound by the same restrictions. Molecular solids are characterized by strong covalent intramolecular bonds but weak van der Waals (vdW) intermolecular bonds. The overlap between wave functions centered on neighboring molecules is small, leading to weak intermolecular electronic coupling. The electronic and optical properties of organic molecular films derive therefore, in first approximation, from those of the closed-shell molecular moieties. They are much less affected by structural defects or lack

of long-range molecular order than in inorganic solids, adding considerable flexibility in device design and processing. A large variety of molecules can be used to realize specific optical or transport applications. Electronic and optical grade films can be deposited from liquid phase (polymers) or by vacuum evaporation (small molecules) on a variety of crystalline or amorphous, organic or inorganic, rigid or flexible substrates without regard for structural match. Multiple layers can be superposed and different molecular materials can be mixed to engineer complex structures and introduce new functionalities while keeping the properties of the constituents essentially unchanged. This must be contrasted to the crystalline perfection required for most optical and optoelectronic devices based on inorganic semiconductors. Of course, the flexibility afforded by molecular films applies to surface and interface studies of these materials as well. For example, the sequence of deposition of various materials can be reversed, e.g. organic-on-metal vs. metal-on-organic, without necessarily deteriorating the intrinsic properties of the materials, thereby increasing the range of meaningful interfaces and phenomena which can be investigated.

Yet, the flexibility enjoyed at the experimental and device processing level comes at a price of considerable complexity at the theoretical level [17,18]. This complexity is inherent to molecular materials and is due to: i. the nature of the constituents of these molecular films, i.e. the large neutral molecular moieties; ii. the relaxation and polarization phenomena that take place in the presence of excess charges; iii. the electronic and vibrational excitations of the molecules; iv. correlation effects and excitonic properties, and v. random disorder due to structural and thermal fluctuations. Electrons and holes are considerably more localized in organic molecular solids than in covalently bound inorganic solids. Energy bands are very narrow and conduction occurs via hopping between molecular sites. The one-electron approximation and rigid band model universally used for wide band "delocalized" inorganic systems is no longer valid for molecular systems. A molecule is a small closed-shell system with relatively few electrons, and the simple addition or removal of a charged particle significantly alters its energy levels. Electronic relaxation, polarization and conformational changes lead to the formation of polarons and other excited states which add to the difficulty in interpreting transport measurements or surface and interface data based on photoemission spectroscopy and related techniques. More will be said on this subject in section IV.

Another important aspect of molecular films, which impacts on the physical nature of their interfaces, is the extent to which the "softness" of the organic materials due to the vdW intermolecular bonds allows diffusion and chemical reaction of metal and other species much deeper into the material than with inorganic semiconductors. Examples of interfaces will be reviewed where metal species diffuse over 1-10 nm into the organic matrix and react with molecules to form an extended interface region of a compound with properties different than those of the pristine material. The issue of molecular interdiffusion at organic-organic heterojunctions is also one that has potential bearing on the performance and lifetime of multilayer devices.

The challenges to fundamental and applied research on organic interfaces are therefore multi-fold. First, it is important to understand which electronic levels are relevant to charge carrier injection at, and transport through, interfaces. Second, a clear understanding of the mechanisms of interface molecular level alignment, leading to predictive models for the energetics of organic interfaces, must be achieved. Third, the

impact of interface chemistry and interfacial layers of new materials on injection and transport characteristics must be clearly established. Finally, methods for interface modifications must be developed in order to achieve systematic and predictive improvement of interfaces. This chapter reviews the work done by our group in some of these research areas and, when possible, attempts to draw general conclusions regarding these interfaces. Section II gives a brief review of experimental methods. Section III summarizes our work on metal-organic and organic-organic interfaces. Section IV addresses the controversial issue of the definition and determination of transport levels in organic molecular solids. The chapter concludes with section V.

## II. Experimental approach

The experiments described in this review, including the deposition of all organic and metallic thin films, were performed in ultra-high vacuum (UHV) at pressures of $10^{-9}$-$10^{-10}$ Torr or below. These conditions are sometimes regarded as remote from the conditions under which organic thin films are being and will be processed for commercial applications. However, UHV processing permits investigations of fundamental interface properties designed to extract information related to the intrinsic nature of the materials under investigation rather than to extrinsic factors such as contamination, known to affect organics and metals used in devices. A specific example of the importance of looking at "clean" interfaces in order to understand the physics of organic-metal interfaces is discussed at the end of section III.3 in the context of the Mg/$Alq_3$ interface [19]. This chapter also focuses exclusively on vacuum evaporated thin films of π-conjugated molecules that can be easily sublimated and condensed in UHV. These organic materials are purified via multiple cycles of sublimation prior to being loaded in the UHV deposition chamber. The chemical structures of the molecules discussed in this review are given in Fig. 2.

The principle group of investigation techniques used in this work is photoemission spectroscopy. Ultra-violet photoemission spectroscopy (UPS) is used to investigate the valence states of the organic and inorganic films, in particular the evolution of the electronic structure around the highest occupied molecular orbital (HOMO) upon formation of interfaces. Photons are produced by synchrotron radiation or by a helium discharge lamp that provides light at 21.22 eV (HeI) and 40.8 eV (HeII). A typical HeI valence spectrum of an organic thin film, measured here from PTCBI (3,4,9,10-perylenetetracarboxylic bisimidazole) [20] is shown in Fig. 3. The spectrum consists of a broad, low-energy secondary electron peak, which results from inelastically scattered electrons, and several well-defined features related to the density of states of the π-system and σ-bonds of the molecular solid. The highest kinetic energy (lowest binding energy) feature corresponds to the HOMO. The energy of the HOMO is generally referred to the Fermi level, measured separately on a metallic electrode. The low-energy edge of the secondary electron peak, i.e. the photoemission cut-off, corresponds to the vacuum level ($E_{vac}$) of the molecular film. The ionization energy (IE) is defined as the energy difference between $E_{vac}$ and the leading edge of the HOMO peak. It is given by

$$IE = h\nu - W$$

where $h\nu$ is the photon energy and $W$ is the total width of the valence spectrum measured from the leading edge of the HOMO peak to the photoemission cut-off (Fig. 3). The shift of the photoemission cut-off upon formation of an interface, corrected for eventual "band bending"-induced shift of the molecular levels, leads to the determination of the dipole barriers (see next section). The typical energy resolution achieved in our UPS system is 150 meV.

The other photoemission technique extensively used in our work on organic interfaces is X-ray photoemission spectroscopy (XPS). XPS probes the core level binding energy of atoms at and near the interface and provides information on chemistry. We use the K$\alpha$ line from an aluminum anode (1486 eV) and the M$\zeta$ line from a zirconium anode (151 eV). The low kinetic energy of electrons photoexcited by the latter provides for a very surface sensitive chemical probe. Both photon lines produce spectra with energy resolution of the order of 0.5 eV.

An important aspect of our work concerns the study of empty states in the energy region of the lowest unoccupied molecular orbital (LUMO) in organic films and at interfaces via inverse photoemission spectroscopy (IPES). IPES is performed in the isochromat mode, by varying the electron energy while keeping the energy of the detected photons fixed. The system, which has been described in details in previous publications [21], has a resolution of 0.5 eV. One of the main concerns with IPES is whether electron-beam-induced deterioration and/or charging occurs in the organic film. Typical experiments reported in this review were performed using small incident electron current densities in the range of $\sim 10^{-7} - 10^{-4}$ A/cm$^2$. Decreasing the current at the expense of the count rate is generally found to result in superior data. The analysis of our IPES data involves standard non-linear least-squares fitting techniques and background subtraction. The interested reader is referred to previous publications for more details [21-23].

Finally, the relationship between the electronic structure, the chemistry and the charge carrier injection characteristics at organic interfaces under investigation is established via current-voltage (I-V) measurements on small devices grown and measured in UHV. The complete in-situ process eliminates eventual effects of cathode oxidation and deterioration of the organic layer in air on the transport characteristics.

## III. Electron and hole barriers at organic interfaces

### *A. Organic-on-metal interfaces: molecular level alignment and interface dipoles*

Understanding the mechanisms that control the energetics of interfaces, in particular the magnitude of energy barriers between the Fermi level ($E_F$) and the HOMO (LUMO) levels across interfaces, has been one of the main challenges to surface and interface studies of organic thin films over the past few years. These energy barriers determine the injection of carriers across interfaces. In that respect, it is useful to briefly reconsider the situation encountered with inorganic semiconductors. Inorganic semiconductor interfaces are controlled by intrinsic and extrinsic electronic gap states. Intrinsic states, like metal-induced gap states at metal-semiconductor interfaces [24] are

the natural consequence of the loss of three-dimensional periodicity on the band structure of the two materials and of the boundary conditions between them, such as interfacial bonds and atomic structure. On the other hand, extrinsic states result from structural defects or chemistry-induced defects that are formed at interfaces [25,26]. Both types of states affect the electronic structure of the interface, as seen for example in the complex dependence of the Schottky barrier height on the metal work function at inorganic semiconductor interfaces [24]. The relative positions of energy levels across inorganic interfaces are controlled by the occupation of these interface states, which gives rise to charge exchange and dipole barriers, as depicted in Fig. 4b for a metal-semiconductor interface.

Because of the "closed shell" nature of molecules and their weak vdW intermolecular bonding, organic molecular semiconductor interfaces had been expected to form weakly interacting boundaries with weak interface bonds and no electronically active defects, leading to interfaces without gap states. Under such conditions, the relative position of molecular levels across the interface would be obtained by simple alignment of the vacuum levels of the two solids, as depicted in Fig. 4a. This situation, which is the equivalent of the Schottky-Mott limit [27] in metal-semiconductor interfaces and of the Anderson rule [28] for semiconductor heterojunctions, was widely assumed to be correct in the literature on organic devices. Recent investigations have now firmly demonstrated that this is rarely the case at metal-organic interfaces [29-38]. Interface dipole barriers with magnitudes greater than 1.0 eV have been seen to introduce discontinuities in the vacuum level across interfaces and cause substantial departure from the simple Schottky-Mott limit (Fig. 4b). Figure 5 shows UPS spectra taken upon formation of the interface between α-NPD (N,N'-diphenyl-N,N'-bis(l-naphthyl)-l,l'biphenyl-4,4''diamine) and Au, which clearly demonstrates this point. The schematic energy diagram of the interface (bottom panel) shows: i. the hole injection barrier measured from the energy difference between the HOMO of the organic film at the interface and the $E_F$ of the substrate in the UPS spectrum (top right panel); ii. the 1.2 eV interface dipole barrier deduced from the abrupt shift of the onset of photoemission (top left panel) upon deposition of the first layer of organic molecules. Neglecting the dipole in this case would introduce a rather large error in the evaluation of the electron or hole injection barriers.

Figure 6 summarizes (a) the position of $E_F$ and (b) the dipole barriers vs. metal work function measured in our laboratory via photoemission spectroscopy for a series of organic-on-metal interfaces. A positive dipole in Fig. 6b indicates a vacuum level drop from the metal into the organic film (identical to the situation depicted in Fig. 4), suggestive of an electron transfer from the organic film to the metal. Alternatively, a negative dipole corresponds to a rise in the vacuum level, indicative of an electron transfer from the metal to the organic. The dipole barriers also appear in Fig. 6a as the vertical segments around each measured point. The dashed lines in panel (a) represent the position that $E_F$ would occupy if these interfaces did follow the Schottky-Mott limit. Also indicated on each plot is the *S* parameter, which gives a measure of how much the energy barrier varies as a function of metal work function (*S*=1 for the Schottky-Mott limit).

Two remarks should be made here. First, the interfaces represented in Fig. 6 were formed by deposition of the organic film on the metal surface, i.e. organic-on-metal

(O/M). This deposition sequence generally leads to a more abrupt interface than the reverse sequence, i.e. metal-on-organic (M/O). The O/M interface allows a more straightforward investigation of the fundamental mechanisms that operate at these interfaces, in particular with respect to molecular level alignment. The reverse deposition sequence is exceedingly important as well, especially in the context of devices, but often leads to diffused interfaces that are more difficult to model. More will be said on this subject in the next section. The second remark concerns the energy gap of each organic film. The energy difference between the two horizontal lines marking the HOMO and LUMO levels was arbitrarily set equal to the optical absorption gap of the material and not to the more appropriate "transport" gap (discussed in detail section IV), which is to be used when discussing energy barriers for charge carrier injection. This approximation, however, does not affect the following discussion.

The obvious conclusion from these data is that the rule of vacuum level alignment breaks down for most of these interfaces. This conclusion was reached early on by Seki and co-workers [29-31] and was subsequently confirmed in a number of experiments by our group [19,20,33-36] and others [37,38]. It raises two key questions: i. Why is the Schottky-Mott rule not respected, in particular in seemingly simple cases where the work function of the metal falls deep between the electron affinity and ionization energy of the semiconductor? ii. What is (are) the mechanism(s) that control molecular level alignment and formation of interface dipole barriers?

In cases where the work function of the metal is smaller than the electron affinity (EA) of the organic solid, like PTCDA on Mg, In or Sn, PTCBI on Mg and Ag and $F_{16}$CuPc on Mg and Al, a simple vacuum level alignment would lead to an interface where $E_F$ is *very close* to or *above* the LUMO of the organic, a clearly untenable situation. Electron transfer from the metal to the organic solid occurs in order to raise the potential of the organic molecular solid and eventually stop the net flow of electrons. In equilibrium, $E_F$ is stabilized *below* the LUMO at the interface. The electron transfer from the metal to the interface molecules gives rise to a *negative* dipole (Fig. 6b) and to occupied states in the gap of the organic semiconductor. All but one of the seven interfaces mentioned above are reactive and the gap states originate from chemistry as well as charge transfer, as will be discussed below in the case of $Alq_3$/Mg. PTCBI/Ag, however, displays no evidence of chemical reaction. Bauschlicher *et al.* [39] have studied the interaction of transition-metal ions with benzene and found that the $Ag^+$ ion forms a weak π-complex. The optimized structure consists of a virtually undisturbed benzene ring with the $Ag^+$ ion relatively far from the C atoms. The aromaticity of the benzene ring is not disturbed, consistent with our observations of bulk-like PTCBI molecular features at the lowest coverages and with the fact that molecular level separations remain constant ± 0.1 eV as a function of film thickness (Fig. 7). In this case, the gap states correspond to an electron transfer from the metal to the LUMO level of the molecule, which induces a re-conformation of the molecule. The result is referred to as polaron (singly occupied) or bipolaron (doubly occupied). At the PTCBI/Ag interface, the two levels that peak above the HOMO at ~0.6 eV and 1.6 eV below $E_F$ are tentatively attributed to bipolaron-like and polaron-like states, respectively [20].

The second type of interface, for which the metal work function ranges between EA and IE of the organic solid, is more complex and diverse. At these interfaces, the

molecular level alignment depends on various bulk and interface characteristics, such as the possibility of moving $E_F$ across the gap of the organic material, the appearance of interface electronic states, and the formation of chemical bonds across the interface. A relatively simple situation emerges when gap states or other mechanisms *inherent to the organic material* restrict the position of $E_F$ in the gap in the bulk and at the surface of the organic film. In order to reach thermodynamic equilibrium, the interface develops a dipole barrier equal to the difference between the metal work function and the organic work function. This is precisely the situation encountered with PTCDA and PTCBI on Au. If the Schottky-Mott rule was valid, the 5.2 eV Au work function should lead to an $E_F$ position deeper in the gap at the interface than experimentally observed. However, UPS measurements on PTCDA [40-43] and PTCBI [20] films of various thicknesses deposited on a variety of metallic and semiconducting substrates consistently show that the Fermi level is "pinned" at a fixed position, roughly 1.5 eV and 1.8 eV above the HOMO for PTCBI and PTCDA films, respectively. These organic molecular materials are nominally undoped and $E_F$ should occupy a much deeper position in the gap. The reason for this "pinning" is unknown, although a small density of impurities or molecular defects could play a role. The consequence is that $E_F$ is consistently pinned high in the gap of these two materials, leading to a *positive* dipole at interfaces with Au.

Besides PTCDA and PTCBI on Au, the majority of interfaces presented in Fig. 6 exhibit *positive* dipoles that are perhaps more difficult to justify. In particular, interfaces like CBP and $Alq_3$ on Ag and Au exhibit dipole barriers which are nearly independent of the metal work function, as shown in Fig. 6b. Image-force effects, whereby the charge density of the interface molecule is polarized by the presence of the metal, and redistribution of the metal charge density by the adsorbed molecules, leading to a decrease in the metal work function and an effective drop of the vacuum level upon adsorption of the molecules, have been invoked to explain the sign and fixed magnitude of these barriers. These mechanisms have been recently reviewed by Ishii *et al.* [32]

Another very important mechanism, which is clearly orthogonal to the notion of weakly interacting interfaces and, as such, is reminiscent of mechanisms active at inorganic semiconductor interfaces [24-26], must be brought up to explain the behavior of interfaces like $Alq_3$-on-Mg or $Alq_3$–Al. It is based on chemistry-induced formation of interface defects, which pin the Fermi level and results in the formation of a a dipole. Our group reported three years ago the formation of gap states upon deposition of Mg on $Alq_3$ [44]. We recently reported the formation of similar gap states for the reverse deposition sequence, i.e. $Alq_3$ on Mg and Al [45] (Fig. 8a). These states result from the exothermic formation of an organometallic complex in which the metal atom attaches to the pyridil side of the quinolate ligand of the molecule [46]. The reaction is favorable due to the tendency of Mg and Al to form covalent bonds with carbon. More will be said on this reaction in the next section dedicated to metal-on-organic interfaces. In the organic-on-metal case, metal atoms do not diffuse into the organic film and the reaction is limited to the first molecular layer. Yet, the reaction product and resulting electronic states are similar to those obtained for Mg or Al on $Alq_3$. These chemistry-induced states are responsible for establishing the interface energetics, i.e. the position of the HOMO relative to $E_F$, early in the deposition sequence. They are filled and force $E_F$ in the upper part of the gap. The positive dipole barrier, i.e. 0.7 eV and 0.9 eV for $Alq_3$ on Mg and Al, respectively, results from an electron transfer from the interface organometallic complex

(i.e. the gap states) to the metal (Fig. 8b). A simple calculation based on a 10Å metal-molecule distance and a dielectric constant of ~3 shows that about 10% of the gap states need to be ionized to sustain the observed dipole. All other states remain occupied, and thus detectable via UPS (Fig. 8a). It is likely that such defect- or chemistry-induced states play a predominant role in determining the molecular level alignment at reactive interfaces. The next section will emphasize the role of these states in inducing "band bending" and establishing barriers at metal-on-organic interfaces.

### *B. Metal-on-organic (M/O) interfaces: chemistry, interdiffusion and barriers*

Thin film organic devices like OLEDs comprise several organic films sandwiched between an anode and a cathode. Future devices will likely include stacked structures in which multiple O/M and M/O interfaces will coexist. M/O interfaces are typically formed by vacuum evaporation or sputtering of a metal on the organic film. In general, M/O interfaces are structurally and chemically more complex than their O/M counterparts. Whereas O/M interfaces are abrupt with the metal-molecule interaction limited to the first molecular layer, isolated metal atoms evaporated on an organic surface are chemically more active and able to diffuse deeper into the molecular matrix. Diffusion plus chemical reaction lead to the formation of extended regions comprising new metal-organic molecular complexes with a different electronic structure than the bulk of the organic film. Determining the chemical structure of such interfaces is exceedingly important for controlling and modeling electronic properties and injection characteristics of the interface regions.

A classic example of metal diffusion into a molecular film is that of In deposited on PTCDA. Synchrotron radiation soft X-ray photoemission spectroscopy brings direct evidence of rapid room temperature diffusion of In over several hundred angstroms of organic film [47-49]. The evolution (or lack thereof) of the In(4d) core level, the highly oxidized state of the metal atoms and the absence of metallic line shape up during the deposition of the first 100-200Å of metal (Fig. 9a) demonstrate that In does not accumulate on top of the organic film. The oxidized state of the metal atom and the elimination of the satellite peak of the C(1s) core level of the molecule (Fig. 9b), attributed to the carbonyl C (bound to oxygen), show that In attaches to the end groups of the molecule. Finally, the large density of electronic gap states induced by the deposition of as little as 1Å In (Fig. 9c) is a strong indication of the profound modification of electronic structure of the organic layer throughout the interface region. Theory shows that up to four In atoms attach to the molecule (Fig. 9c) and links the gap states to the charge density of the new molecular entity and occupation of the former LUMO of the molecule by the charge transferred from In [50]. Sn, Al and Ti are found to behave similarly on PTCDA, although the diffusion of these species is somewhat limited as compared to In [48,49]. Fig. 10 shows the composite photoemission-inverse photoemission spectra recorded from PTCDA as a function of In deposition. Note the position of $E_F$ "pinned" in the upper part of the gap of pristine PTCDA, as discussed in the previous section. The drastic narrowing of the gap due to the appearance of the In-induced states is indicative of the profound modification of the electronic structure of the organic material with respect to that of the pristine molecular solid. Understanding these changes is the key to understanding the electrical properties of this interface.

The remainder of this section summarizes the state of understanding of the chemistry and electronic structure of a couple of technologically important M/O interfaces, i.e. Mg and Al on $Alq_3$. $Alq_3$ is one of the most extensively used electron transport and emissive layers for OLEDs. Mg and, to a lesser degree, Al are low work function metals used for electron-injecting cathodes on $Alq_3$ films. Several groups have therefore investigated these interfaces [51-55] and have reported various interactions ranging from simple metal-to-molecule charge exchange to metal-O coordination at the center of the molecule. Our work, summarized below, shows how complex the chemical interaction resulting in the formation of an organometallic complex can be. Also discussed are the results from carrier injection experiments designed to investigate the respective behaviors of $Mg/Alq_3$ and $Alq_3/Mg$ interfaces.

The tendency of Mg and Al to form covalent metal-C bonds [56] and the affinity of these metal atoms for O lead to considerable interface chemical interaction upon deposition on $Alq_3$. The reaction results in a complex set of chemical shifts in the XPS data measured for Mg deposited on a 100Å $Alq_3$ film (Fig. 11). Mg is "oxidized" during the initial stages of deposition, resulting in a dominant high binding energy (BE) component of Mg(2p). The metallic Mg component signaling accumulation of the metal on the organic film becomes dominant only following the deposition of 32Å and 64Å. The C(1s) undergoes a 0.6 eV shift to higher BE with the first Mg deposition, and its position and shape remain basically unchanged thereafter. The same shift is observed on the N(1s) and O(1s) core levels. It represents a rigid shift analogous to band bending induced by the deposition of a metal on an inorganic semiconductor surface. However, unlike the C(1s) peak, the N(1s) and O(1s) peaks broaden considerably. The N(1s) core level develops a *low* BE component at 399.1eV (~ 1.8eV chemical shift), which corresponds to an excess electronic charge on and around N. On the other hand, the O(1s) core level develops a *high* BE component. The 1.4eV chemical shift corresponds to a net withdrawal of negative charge from oxygen. Finally, the Al(2p) undergoes a 1eV shift to high BE, which corresponds to a net chemical shift of 0.4eV to *higher* BE over and beyond the ubiquitous 0.6eV "band bending" shift. The peak areas of the O(1s), C(1s), N(1s) and Al(2p) remain basically unchanged up to a nominal coverage of 16Å, confirming that Mg does not initially accumulate on the surface of the organic film. The increase in the total area of the Mg(2p) peak demonstrates that the overall metal atom concentration does increase, and thus indicates that the metal atoms diffuse into the film. Eventually, reaction sites are depleted, Mg begins to accumulate at the surface, and the intensity of the various $Alq_3$ signals is attenuated.

The key result in terms of interface chemical structure is the opposite sign of the O(1s) and Al(2p) vs. N(1s) chemical shifts, which is incompatible with a simple charge donation from the metal atom to the molecule. It signals the formation of an organometallic complex. In that regard, the results are quite different than for Ca, K or Li on $Alq_3$. These latter elements form considerably weaker bonds with C [57] and undergo only a charge exchange with the molecule, leading to a metal cation-molecular anion complex, consistent with XPS chemical shifts observed experimentally for the Ca-$Alq_3$ system [51]. In the $Mg/Alq_3$ case, Mg forms a covalent bond with C at the pyridyl ring of the quinolate ligand. Mg donates a charge to the $Alq_3$ LUMO, which is maximized on the pyridyl ring and at N [22]. The result is a *high* BE component of

Mg(2p) (oxidized species) and a *low* BE component of N(1s). The Mg atom further coordinates as an electrophile to a quinolate O of the same or of a neighboring molecule, and in the process pulls charge away from O. This results in *high* BE components on O(1s) and on the 2p level of the central Al atom of the molecule to which O is directly bound. The model of the Mg-$Alq_3$ complex is presented in Fig. 12. The deposition of Al on $Alq_3$ leads to a very similar set of chemical shifts, consistent with the similar tendency of Al to form covalent Al-C bonds. The chemical model developed above therefore applies to the latter interface as well [45].

The UPS data provide information on the electronic structure of the Mg/$Alq_3$ interface. The initial deposition of Mg attenuates the $Alq_3$ features, consistent with the chemistry-induced "smearing" of the top molecular layers of the organic film (Fig. 13). All the molecular levels shift by 0.6eV toward *higher* BE and remain at the same energy thereafter, in agreement with the 0.6eV band bending shift deduced from the XPS data. The origin of this shift becomes clear when considering the gap states induced by the Mg deposition at ~1.9eV above the original HOMO. These filled states, which correspond to the organometallic complex formed in the top layers of the film, push $E_F$ upwards in the gap by 0.6 eV with respect to its original position at 2.1 eV above the leading edge of the HOMO. The shift corresponds to the "band bending" depicted in Fig. 13. The spatial extend of the band bending in not known in the present case, although the width of the reacted interface region is believed to be limited to 5-10 molecular planes.

In relation to the discussion given in the previous section, it is interesting to note that the final positions of the $Alq_3$ HOMO with respect to $E_F$ are nearly identical at the O/M and M/O interfaces, suggesting that the electron and hole injection barriers are identical ±0.1 eV as well. Given this identity, it is important to understand whether the presence of a wider reacted interface in the M/O case plays a role in the injection process. It is generally believed that a depth distribution of the type of gap states observed at these interfaces could facilitate current injection via a "stepping stone" effect [58], leading to a higher injection current from the metal-on-top interface. Such an asymmetry was believed to occur in nominally symmetric Mg:Ag/$Alq_3$/Mg:Ag structures (Fig. 14a), based on I-V measurements showing that the current injected from the metal-on-top electrode was two to three orders of magnitude larger at identical bias than the current injected from the bottom electrode [59] (Fig. 14b). This asymmetry, however, was later shown to be due to contamination effects. Mg/$Alq_3$/Mg and Al/$Alq_3$/Al sandwich structures fabricated and tested in UHV ($10^{-9}$-$10^{-10}$ Torr) showed nearly perfect symmetry of the currents injected from the top or bottom electrodes [19] (Fig. 14c,d), consistent with the identical barriers measured via photoemission and reported above. The previously reported asymmetry was shown via XPS to be due to a blocking oxide layer accumulated on the reactive Mg electrode prior to deposition of $Alq_3$ in a $10^{-6}$ Torr vacuum.

The symmetry exhibited by these interfaces does not invalidate the notion that "stepping stones", provided by chemical reaction or other means, can help the injection process. The lack of effect in the two examples discussed above is merely due to the fact that the states that could play a role in the extended M/O reacted region are filled states and thus do not participate in the electron injection process. The situation is clearly different if the interface states are relevant to conduction. For example, we have

demonstrated a remarkable increase in hole injection from indium tin oxide (ITO) into α-NPD using an ultra-thin (30Å) layer of a compound (i.e. CuPc) exhibiting a hole-conduction level at intermediate energy between the $E_F$ of ITO and the HOMO of α-NPD [60] (Fig. 15). The "stepping stone" effect is clearly active in such a case.

As a final remark, Fig. 14e shows that electron injection into $Alq_3$ obtained from both top and bottom Mg:Ag electrodes is superior to that obtained from pure Mg electrodes. Although recognized early on by OLED practitioners [1] and believed to be due to improvement in morphology and stability of Mg by Ag, this behavior has not yet been fully explained to date.

### *C. Organic-organic heterojunctions: molecular level alignment*

The electronic structure of organic-organic (OO) heterojunctions is exceedingly important for multi-layer organic devices. High efficiency OLEDs made of vacuum-deposited molecular films often comprise an electron transport layer (ETL), a hole transport layer (HTL) and an emissive layer. Energetically efficient transport of electrons and holes across boundaries between these organic layers presupposes a favorable interface arrangement of molecular levels. Hole- or exciton-blocking layers are often inserted near one of the contacts of the device to restrict exciton formation and recombination to one layer of the device, or to prevent non-radiative exciton recombination at the metal interfaces. The proper function of these various blocking layers in the device depends on the energy barriers they introduce in the path of the carriers. Understanding molecular level alignment at OO interfaces is therefore highly relevant to modeling device behavior.

Figure 16 shows the evolution of the UPS spectra of the HOMO energy region during the formation of the α-NPD-on-CuPc heterojunction [60,61]. The two HOMOs coexist at intermediate coverage, with the intensity of the CuPc HOMO diminishing as the α-NPD HOMO intensity increases at higher coverage. The CuPc base layer is not completely suppressed even at a nominal α-NPD thickness of 48 Å, indicating some degree of three-dimensional island growth. This allows a direct and accurate measurement of the HOMO-HOMO offset up to an α-NPD coverage of several molecular layers, sufficient to insure that the electronic structure of the overlayer film is fully developed.

A summary of the alignment of organic levels at twelve organic/organic heterointerfaces is presented in Fig. 17. Within the experimental error of 0.1 eV, the molecular level alignment follows the vacuum alignment rule in a majority of cases [61-63]. This is not surprising, considering the closed-shell nature of the molecules that comprise both constituents of the heterointerface. Charge exchange, chemical bonds and chemistry-induced defects of the type encountered at metal-organic interfaces are not expected to occur at OO heterointerfaces. Some of these OO interfaces, however, exhibit larger dipoles: CuPc/PTCDA (0.4 eV) [36], PTCDA/$Alq_3$ (-0.5 eV) [42-43], α-NPD/$Alq_3$ (-0.25 eV) [43], and BCP/PTCBI (0.4 eV) [61] where the dipole is defined as positive when the vacuum level of the second material is at a higher energy that the first. Ishii *et al* [64] recognized that dipoles occur at heterointerfaces between materials of greatly

differing ionization energies and electron affinities, which are referred to as donor/acceptor interfaces. In such cases, a partial charge is expected to be transferred from the low ionization energy constituent to the high electron affinity molecule. This argument, which is also at the basis of the work on molecular doping [65,66], may be used to explain the interface dipoles measured between the high electron affinity molecule, PTCDA, and the lower ionization energy molecules, CuPc and $Alq_3$. However, the same argument would predict that the PTCDA/α-NPD interface should also contain a strong dipole, given that α-NPD has a lower ionization energy and electron affinity as compared to $Alq_3$. This prediction contradicts the observation of a negligible dipole at this interface. Three of the materials leading to interfaces with significant dipoles also exhibit limited ranges of $E_F$ movement at heterointerfaces (PTCDA, PTCBI, BCP). As noted in the previous sections, $E_F$ may be "pinned" due to defects or impurities, and the dipoles are the result of (de)populating a high density of impurity states near the interfaces. Yet, the 0.5 eV dipole observed at the PTCDA/$Alq_3$ interface cannot be explained on this basis, given the above observation that the Fermi level is relatively free to move within the $Alq_3$ gap (Fig. 6). Considering the mechanisms suggested above, and the counter examples, one must conclude at this point that neither of the suggested mechanisms for dipole formation at organic/organic heterointerfaces is sufficient to explain all of the observed behaviors. Other OO interfaces such as PTCDA/ZnPc (zinc phthalocyanine) [67], PTCDA/ClInPc (chloroindium phthalocyanine) [67], CuPc/NPB (naphthyl-substituted benzidine derivative) [68], $Alq_3$/NPB [69] and $Alq_3$/TPD [70] have been investigated and found to exhibit dipoles ranging between 0 and 0.25 eV. The overwhelming conclusion is therefore that interface dipole barriers at OO heterojunctions are, if significant at all, smaller than at OM interfaces. The assumption of vacuum level alignment, which is widely used at present in the literature for device modeling, is not expected to cause the same level of error than at OM interfaces.

The situation is somewhat different at organic/inorganic semiconductor interfaces. Figure 18 shows energy level alignment measured for α-NPD and CuPc on InP(110) and for PTCDA on GaAs(100). The dipole barrier is substantial (magnitude ≥ 0.4 eV) at each interface [71]. Several mechanisms contribute to this apparent difference with OO interfaces. First, the InP(110) and GaAs(100) surfaces are known to exhibit rather strong near mid-gap $E_F$ pinning following deposition of almost any ad-atom or ad-molecule. The alignment of $E_F$ across these interfaces is therefore more constrained than at OO interfaces. Second, the GaAs and InP band gaps are smaller than those of all three organics. The ionization energy of GaAs (5.56 eV) is significantly smaller than that of PTCDA, placing the inorganic valence band top relatively close to the PTCDA LUMO, and the electron affinity of InP (4.45 eV) is smaller but close to the ionization energy of CuPc, leading to possible mixing of states and charge transfer. The dipole barriers measured at all three interfaces indeed tend to re-align the energy levels to decrease mixing and charge transfer. Third, dangling bonds at the inorganic semiconductor surfaces lead to stronger chemical bonding with the molecules than exist across OO interfaces, and thus allow more readily charge transfer and formation of dipoles. In that sense, organic/inorganic semiconductor interfaces are closer to MO interfaces than to OO interfaces.

## IV. Transport gap and exciton binding energy in molecular films

This final section focuses on the difficult task of reconciling energy levels and gaps measured via PES and IPES, which we will argue to be relevant to carrier injection and transport in molecular solids, with energy levels and gaps measured via optical absorption and other means. This task, which is still largely ignored in today's literature on devices, is key to the development of realistic interface transport models.

The complexity of the relaxation and polarization effects, and electronic and vibrational excitations in the basic molecular unit of the organic films, which we alluded to in the introduction, brings an important question with regard to the assignment of energy levels of charge carriers. Energy levels and charge carrier transport in standard inorganic semiconductors are well described in terms of delocalized states and the single-band approximation. Because of delocalization and efficient screening, exciton binding energies are small. The transport gap $E_t$, also known as the single particle gap, defined as the minimum energy of formation of a separated free electron and hole in the solid, is within a few meV of the optical gap $E_{opt}$. $E_{opt}$ corresponds to the onset of optical absorption.

The situation is fundamentally different in molecular solids, in which localization and polarization dominate the physics of charged excitation and transport [17,18,72]. These solids exhibit small intermolecular overlaps and large polarizabilities involving charges and induced dipoles [18, 73]. The optical gap, $E_{opt}$, corresponds to the formation of a Frenkel or charge transfer (CT) exciton, with the electron and hole on the same or adjacent molecules, respectively, rather than to a band-to-band transition [74]. Because of the weak screening and strong electron-hole coulomb interaction, $E_{opt}$ is expected to be several tenths of an eV below $E_t$. Thus $E_t$ does not follow from optical measurements, unlike in inorganic semiconductors, and is basically unknown unless independently determined. The molecular levels that are relevant to charge injection and transport are therefore poorly understood as well. Yet, knowledge of these levels is essential for constructing reliable energy diagrams for carrier injection and transport.

Recent measurements using electron energy loss spectroscopy have provided an interesting correlation between the size of the exciton and the size of the excited molecule for a number of π-conjugated molecules [75]. This trend is consistent with previous reports of small exciton binding energy (200 meV or less) in conjugated polymers where the excitation is delocalized over long chains [72,76], and large exciton binding energies ($\geq$ 1.5 eV) in small molecules like $C_{60}$ [77-80]. Yet, the issue of exciton binding energy, $E_t - E_{opt}$, continues to be a rather controversial one. Measurements of $E_t$, which lead to the determination of the exciton binding energy provided that the optical absorption spectrum of this solid is known and understood, can be performed via photoconductivity in the organic film [81], internal photoemission measurement of electron and hole barriers at organic/metal interfaces [82], and the combination of direct and inverse photoemission spectroscopies (PES, IPES) [21,23,77,78].

The combined PES and IPES measurements of the HOMO and LUMO of a molecular film is the equivalent of an experiment in which an electron is removed from a molecule (PES), then added to another (IPES) to form an uncorrelated free electron/hole

pair. It is the measurement of the energy difference between the hole-state and electron-state induced in the process, and the comparison of this difference with the energy of formation of a correlated electron-hole pair, i.e. an exciton, that lead to the exciton binding energy.

A schematic diagram of energy levels of gas phase and condensed phase molecules is given in the bottom of Fig. 19. On the left part of the diagram, the gas phase ionization energy (I) corresponds to the energy difference between the HOMO of the molecule and the vacuum level. The electron affinity (A) is the energy difference between the vacuum level and the LUMO of the molecule (measured via IPES). I and A are reduced and increased, respectively, in the condensed phase by polarization, i.e. the response of the medium to the creation of a molecular ion (illustrated at the top of Fig. 19). Because of the polarization energy ($P_+$) induced on the surrounding medium by the photoinduced hole, the hole energy shifts to lower energy (upward on the electron energy scale) with respect to the HOMO level of the isolated molecule. This polarization includes an *electronic* component, which consists of the response of the electronic charge density of the central and surrounding molecules to the formation of the hole. This response is fast (~$10^{-16}$ s) and accounts for most of the polarization energy [18]. The polarization also includes a *vibronic* component, which corresponds to the new equilibrium geometric configuration of the molecular cation. This component switches on a time scale set by the "breathing" ($a_g$) molecular modes (~$10^{-15}$ - $10^{-14}$ s). The UPS spectrum of the HOMO includes both polarization components and provides therefore a measure of the nearly fully relaxed positive polaron (the missing piece is the lattice relaxation component, which is too slow to be included in the PES process, but is also very small, ~ few tens of meV), which is the relevant hole transport level in the molecular solid. The measured energy level of the nearly fully relaxed positive polaron is labeled $E_P^+$ in Fig. 19. Similarly, the IPES spectrum shows the LUMO shifted by the polarization $P_-$ induced by the presence of the molecular anion. $P_-$ includes components that are conceptually identical, although not necessarily equal in magnitude, to those of $P_+$. The energy level of the nearly fully relaxed negative polaron is labeled $E_P^-$ in Fig. 19.

A comparison between occupied and unoccupied electronic levels measured via PES/IPES and calculated with a semi-empirical Hartree-Fock intermediate neglect of differential overlap method is given in Fig. 20 for α-NPD [22]. Similar agreement was obtained for PTCDA and $Alq_3$, demonstrating in the process that IPES can be used to investigate empty states of a number of organic films without significant electron-beam-induced deterioration of the film. Figure 21 gives the composite PES/IPES spectra for four organic films. From these spectra, the determination of the transport gap $E_t$ requires the consideration of several points. The first addresses the choice of the peak-to-peak HOMO-LUMO gap, rather than the edge-to-edge gap, to evaluate $E_t$. The rationale for this choice is that the HOMO and LUMO peaks measured on the molecular films derive from narrow HOMO and LUMO peak of the gas phase molecule shifted by polarization and broadened by solid state effects and random disorder. Thus the relevant HOMO-LUMO gap is between the peak centroids. Vibrational levels, too closely spaced to be resolved, and perhaps some delocalization of molecular states due to intermolecular wave function overlap, contribute to the widths, but to a lesser extent [83]. Vibrational excitation in PES/IPES will tend to shift both the measured HOMO and LUMO peaks away from the Fermi level. The measured peak-to-peak separation increases by the

Franck-Condon maxima. To correct for this, a 100 meV shift is estimated for each peak and 0.2 eV is subtracted from the PES/IPES gap. Second, the difference between surface and bulk polarizations must be understood and corrected for in the PES/IPES gap. PES and IPES are surface sensitive techniques and, as such, measure hole and electron levels located predominantly in surface molecules. Polarization induced by a surface molecular ion is reduced due to the reduced number of neighboring molecules, leading to a "surface transport gap" which is in fact larger than the bulk transport gap. It is interesting to note that the evaluation of polarization energies using the available gas phase PES data on PTCDA [84], $Alq_3$ [85] and CuPc [86] and our condensed phase PES data lead to identical $P_+$'s equal to 1.15±0.3 eV for all three materials. The correction to obtain the bulk from the surface polarization was experimentally estimated by Salaneck to be around 0.3 eV for a molecule like anthracene [87]. This difference may in fact change in layers of molecules like PTCDA whose in-plane polarization is significantly larger than out-of-plane polarization, thereby increasing the weight of in-plane neighbors relative to the polarization from the plane below the molecule. Understanding the film structure and surface morphology is of course necessary to quantify these differences more precisely. Short of additional information, it is therefore assumed that the surface to bulk difference in polarization is 0.3 eV for the HOMO and 0.3 eV for the LUMO. The total correction from measured HOMO-LUMO gap to the bulk $E_t$, including the 0.2 eV for vibrational excitation, is therefore 0.8 eV, leading to the numbers given in the second column of Table 1. Note that the uncertainty on $E_t$ is large (±0.4 eV), given the approximations stated above. The third column gives $E_{opt}$, defined as the energy corresponding to the maximum of the absorption peak. The last column gives $E_t$-$E_{opt}$, the charge separation energy or *exciton binding energy* in the molecular film.

The more delocalized π-systems like PTCDA exhibit bulk electron-hole binding energies around 0.6 eV, which is in relatively good agreement with the 0.8 eV result reported for pentacene [88]. The 0.4 eV result for α-6T is also in line with the 0.2 eV reported for α-6T [75]. The latter molecule is significantly longer than α-6T (32Å vs. 23Å) and sustains a more extended exciton (28Å vs. 14Å) with lower binding energy. The binding energy in α-NPD and $Alq_3$ is significantly larger and equal to 1.0 and 1.4 eV, respectively. Note that the $Alq_3$ result is incompatible with the 0.3 eV value based on internal photoemission [88]. The reason for this discrepancy is unclear at this point. It is somewhat surprising, however, given the good agreement between the resulting electron barriers at this interface (see below). These results for $E_t$ are for conjugated molecules with transport or device applications as thin films. As expected, the transport gap is more accurately known in organic crystals than in amorphous films. Crystalline polymers based on substituted polydiacetylenes (PDAs) have $E_t$ = 2.5 eV and 0-0 peak of $E_{opt}$ = 2.0 eV, with small variations with substituents and temperature [89]. These binding energies are consistent with the above estimates for PTCDA, α-6T and CuPc; their 0-0 peak just above or below 2 eV suggests comparable delocalization and polarizabilities. Anthracene crystals have $E_t$ = 4.1 eV and $E_{opt}$ = 3.1 eV [17], in accord with a smaller π-system and cation-anion separation. Comparison with α-NPD is rough, however, because that molecule is not planar. The binding of naphthalene is large [18] and comparable to $Alq_3$, whose quinolate ligands also contain two rings. The anion and cation charges in adjacent $Alq_3$ are largely localized on individual ligands. We note that these encouraging

comparisons with crystal data do not extend to amorphous films of conjugated polymers, where $E_{opt}$ is known but different techniques for extracting $E_t$ yield binding energies ranging from a few kT to over 1 eV [74].

Beyond the evaluation of the exciton binding energy, the impact of this work on interfaces of interest here should be to provide more accurate barriers for electron and hole injection. Indeed, the position of the hole state relative to the Fermi level at a MO interface or to another hole-state at a OO interface, i.e. the hole barrier, is known from PES. As argued above, the determination of the electron barrier cannot be inferred from the hole barrier and the optical gap, and requires IPES or internal photoemission measurements or knowledge of the transport gap $E_t$. The sum of the electron and hole barriers is the single-particle or transport gap of the material. Figure 22 gives a tentative example of gap correction for the Mg/$Alq_3$ interface. $E_F$ is measured at about 2.7-2.8 eV above the leading edge of the HOMO peak (Fig. 6a). Using the optical gap and neglecting the exciton binding energy (Fig. 22, left) makes the electron injection barrier (leading edge of the LUMO peak – $E_F$) extremely small ($\leq$ 0.1 eV). $E_t$ defined above is the energy gap between the centroids of the HOMO and LUMO peaks. The gap between the edges of the HOMO and LUMO peaks is smaller than $E_t$ by roughly twice the base width of the peaks (Fig. 22, right). The composite $Alq_3$ PES/IPES data [23] gives an edge gap of about 3.7-3.8 eV. Using the more appropriate transport gap increases the energy difference between the $E_F$ and the edge of the LUMO peak to about 0.9 eV, more in line with the 0.6 eV value based on internal photoemission [82] and with current thinking that transport at this interface is injection limited.

## V. Conclusions

Surface and interface techniques have been shown time and again to be extremely powerful for unraveling fundamental problems related to semiconductor heterointerfaces. The work done over the past decade on interfaces of molecular films certainly confirm the importance and validity of a surface/interface approach. The overwhelming conclusions of our work and that of others are that organic interfaces are chemically and electronically more complex and varied than initially perceived. In the context of an emerging technology based on thin film devices, interfaces continue to play a disproportionately important role, as they often constitute the bottleneck to the injection and transport of charge carriers. In the same time, the flexibility afforded by organic molecular films in terms of modes and conditions of deposition, chemical modification of materials, molecular mixing and doping are opening a number of avenues for modifying and improving interfaces in ways which cannot be applied to inorganic semiconductors. The role of surface/interface science in taking advantage of this flexibility will be extremely important.

### Acknowledgements

Several people participated in the experimental work and in the theoretical analysis of the data reviewed in this chapter. Many thanks are due to Drs. Yutaka Hirose,

Aparna Rajagopal and Chih-I Wu and Ms. Weiying Gao for their PES and IPES work on organic interfaces, to Prof. Jean-Luc Brédas and Drs. Jerôme Cornil and Denis dos Santos for their collaboration on filled and empty state calculations, to Prof. Zoltan Soos for his collaboration on the problem of electron-hole separation energy, and to Prof. Steve Forrest and his group for many helpful discussions and generous help in providing organic materials. Support of this work by the MRSEC program of the National Science Foundation (DMR-9809483) and by the New Jersey Center for Optoelectronics is gratefully acknowledged.

**References**


1. C.W. Tang and S.A. VanSlyke, Organic Electroluminescent Diodes, Appl. Phys. Lett. 51, 913 (1987)
2. N.C. Greenham and R.H. Friend, Semiconductor Device Physics of Conjugated Polymers, Solid State Physics, 49, 1 (1995)
3. S.R. Forrest, Ultrathin Organic Films Grown by Organic Molecular Beam Deposition and Related Techniques, Chemical Reviews 97, 1793 (1997)
4. Z. Shen, P.E. Burrows, V. Bulovic, S.R. Forrest and M.E. Thompson, Three-Color, Tunable, Organic Light-Emitting Devices, Science 276, 2009 (1997)
5. Z. Shen, P.E. Burrows, V. Bulovic, S.R. Forrest and M.E. Thompson, Three-Color Tunable, Organic Light-Emitting Devices, Science, 276, 2009 (1997)
6. A.W. Grice, D.D. Bradley, M.T. Bernius, M. Inbasekaran, W.W. Wu and E.P. Woo, High Brightness and Efficiency Blue Light-Emitting Polymer Diodes, Appl. Phys. Lett. 73, 629 (1998)
7. J. Kido and Y. Iizumi, Fabrication of Highly Efficient Organic Electroluminescent Devices, Apl. Phys. Lett. 73, 2721 (1998)
8. V.G. Kozlov, V. Bulovic, P.E. Burrows and S.R. Forrest, Laser Action in Organic Semiconductor Waveguide and Double-Heterostructure Devices, Nature, 389, 362 (1997)
9. J.H. Schön, Ch. Kloc, A. Dodabalapur and B. Batlogg, An Organic Solid State Injection Laser, Science, 289, 599 (2000)
10. A. Dodabalapur, L. Torsi and H.E. Katz, Organic Transistor: Two-Dimensional Transport and Improved Electrical Characteristics, Science, 268, 270 (1995)
11. G. Horowitz, F. Garnier, A. Yassar, R. Hajlaoui and F. Kouki, Field Effect Transistor Made with Sexithiophene Single Crystal, Adv. Mat. 8, 52 (1996)
12. A. Dodabalapur, J. Laquindanum, H.E. Katz and Z. Bao, Complementary Circuits with Organic Transistors, Appl. Phys. Lett. 69, 4227 (1996)
13. Y.Y. Lin, D.J. Gundlach, S.F. Nelson and T.N. Jackson, Stacked Pentacene Layer Organic Thin-Film Transistors with Improved Characteristics, IEEE Elec. Device Lett. 18, 606 (1997)
14. G. Yu, J. Gao, J.C. Hummelen, F. Wudl and A.J. Heeger, Polymer Photovoltaic Cells: Enhanced Efficiencies via a Network of Internal Donor-Acceptor Heterojunctions, Science 270, 1789 (1995)
15. P. Peumans, V. Bulovic and S.R. Forrest, Efficient Photon Harvesting at High Optical Intensities in Ultrathin Organic Double Heterostructure Photovoltaic Diodes, Appl. Phys. Lett. 76, 2650 (2000)
16. W.R. Salaneck, S. Stafström and J.-L. Brédas, Conjugated Polymer Surfaces and Interfaces, Cambridge University Press, 1996

17. M. Pope and C.E. Swenberg, in Electronic Processes in Organic Crystals, Clarendon Press, Oxford University Press, Oxford, New York, 1982

18. E.A. Silinsh and V. Capek, in Organic Molecular Crystals: Interaction, Localization and Transport Phenomena, American Institute of Physics, New York, 1994

19. C. Shen, I.G. Hill and A. Kahn, Role of Electrode Contamination in Electron Injection at Mg:Ag/$Alq_3$ Interfaces, Adv. Mat. 11, 1523 (1999)

20. I.G. Hill, J. Schwartz and A. Kahn, Metal-Dependent Charge Transfer and Chemical Interaction at Interfaces Between 3,4,9,10-Perylenetetracarboxylic Bisimidazole and Gold, Silver and Magnesium, Organic Electronics, 1, 5 (2000)

21. C.I. Wu, Y. Hirose, H. Sirringhaus and A. Kahn, Electron-Hole Interaction Energy in the Organic Molecular Semiconductor PTCDA, Chem. Phys. Lett. 272, 43 (1997)

22. I.G. Hill, A. Kahn, J. Cornill, D.A. dos Santos and J.L. Brédas, Occupied and Unoccupied Electronic Levels in Organic π-Conjugated Molecules: Comparison between Experiment and Theory, Chem. Phys. Lett. 317, 444 (2000)

23. I.G. Hill, A. Kahn, Z.G. Soos and R.A. Pascal Jr., Charge Separation Energy in Films of π-Conjugated Organic Molecules, Chem. Phys. Lett., 327, 181 (2000)

24. W. Mönch, Semiconductor Surfaces and Interfaces, Springer-Verlag: Berlin Heidelberg, 1993 p. 72.

25. E.H. Rhoderick and R.H. Williams, Metal-Semiconductor Contacts, 2nd ed. Oxford, 1988, p. 33

26. L.J. Brillson, The Structure and Properties of Metal-Semiconductor Interfaces, Surf. Sci. Report, 2, 123 (1982)

27. W. Schottky, Halbleitertheorie der Sperrschicht, Natur Wissenshaften, 26, 843 (1938).

28. R.L. Anderson, Experiments on Ge-GaAs Heterojunctions, Sol. State Electron. 5, 341 (1962).

29. H. Ishii and K. Seki, Energy Level Alignment at Organic/Metal Interfaces Studied by UV Photoemission: Breakdown of Traditional Assumption of a Common Vacuum Level at the Interface, IEEE Trans. Electron Devices 44, 1295 (1997)

30. D. Yoshimura, H. Ishii, S. Narioka, M. Sei, T. Miyazaki, Y. Ouchi, S. Hasegawa, Y. Harima, K. Yamashita and K. Seki, The Electronic Structure of Porphyrin/Metal Interfaces Studied by Ultraviolet Photoemission Spectroscopy, J. Electron Spect. Rel. Phenom. 78, 359 (1996)

31. K. Sugiyama, D. Yoshimura, E. Ito, T. Miyazaki, Y. Hamatani, I. Kawamoto, H. Ishii, Y. Ouchi, and K. Seki, Electronic Structure of Organic Carrier Transporting Material / Metal Interfaces as a Model Interface of Electroluminescent Device Studied by UV Photoemission, Synthetic Metals, 86, 2425 (1997)

32. H. Ishii, K. Sugiyama, E. Ito and K. Seki, Energy Level Alignment and Interfacial Electronic Structures at Organic/Metal and Organic/Organic Interfaces, Adv. Mat. 11, 605 (1999)

33. I. Hill, A. Rajagopal, A. Kahn and Y. Hu, Molecular Level Alignment at Organic Semiconductor-Metal Interfaces, Appl. Phys. Lett. 73, 662 (1998)

34. A. Rajagopal, I. Hill and A. Kahn, Electronic Properties of Metal-Organic Interfaces with Application to Electroluminescent Devices, Mol. Crystals and Liquid Crystals A 322, 245 (1998)

35. I. Hill, A. Rajagopal and A. Kahn, Energy level alignment at interfaces between metals and the organic semiconductor 4,4'-N,N'-dicarbazolyl-biphenyl, J. Appl. Phys. 84, 3236 (1998)

36. I.G. Hill and A. Kahn, Interface electronic properties of organic molecular semiconductor interfaces, in Organic Light-Emitting Materials and Devices II, Zakya H. Kafafi Editor, Proceedings of SPIE, Vol. 3476, 168 (1998)

37. S.T. Lee, X.Y. Hou, M.G. Mason and C.W. Tang, Energy Level Alignment at $Alq_3$/Metal Interfaces, Appl. Phys. Lett. 72, 1593 (1998)

38. I.G. Hill, A.J. Mäkinen and Z.H. Kafafi, Initial Stages of Metal/organic Semiconductor Interface Formation, J. Appl. Phys. 88, 889 (2000)

39. W. Bauschlicher, Jr., H. Partridge, and S. R. Langhoff, Theoretical Study of Transition-Metal ions Bond to Benzene, J. Phys. Chem., 96, 3273 (1992)

40. Y. Hirose, W. Chen, E.I. Haskal, S.R. Forrest and A. Kahn, Organic-Inorganic Semiconductor Interface: PTCDA/GaAs(100), Appl. Phys. Lett. 64, 3482 (1994)

41. Y. Hirose, W. Chen, E.I. Haskal, S.R. Forrest and A. Kahn, Structural and Electronic Properties of an Organic/Inorganic Semiconductor Interface: PTCDA/GaAs(100), J. Vac. Sci. Technol. B 12, 2616 (1994)

42. A. Rajagopal and A. Kahn, Molecular Level Offset at the PTCDA/$Alq_3$ Heterojunction, Adv. Mat. 10, 140 (1998)

43. A. Rajagopal, C.I. Wu and A. Kahn, Energy Level Offset at Organic Semiconductor Heterojunctions, J. Appl. Phys. 83, 2649 (1998)

44. A. Rajagopal and A. Kahn, Mg/$Alq_3$ Interfaces: Electronic Structure and Interdiffusion Studied by Photoemission Spectroscopy, J. Appl. Phys. 84, 355 (1998)

45. C. Shen, A. Kahn and J. Schwartz, Chemical and Electrical Properties of Metal and Tris-(8-hydroxy quinoline) Aluminum Interfaces, J. Appl. Phys. (in press)

46. C. Shen, I.G. Hill, A. Kahn and J. Schwartz, Organometallic Chemistry at the Magnesium-tris(8-hydroxyquinolino) Aluminum Interface, J. Am. Chem. Soc. 122, 5391 (2000)

47. Y. Hirose, A. Kahn, V. Aristov, and P. Soukiassian, Chemistry, Diffusion and Electronic Properties of a Metal/Organic Semiconductor Contact: In / PTCDA, Appl. Phys. Lett. 68, 217 (1996)

48. Y. Hirose, A. Kahn, V. Aristov, P. Soukiassian, V. Bulovic and S.R. Forrest, Chemistry and Electronic Properties of Metal/Organic Semiconductor Interfaces: Al, Ti, In, Sn, Ag and Au on PTCDA, Phys. Rev. B 54, 13748 (1996)

49. Y. Hirose, C.I. Wu, A. Kahn, V. Aristov and P. Soukiassian, Chemistry and Electrical Properties of Metal Contacts on an Organic Molecular Semiconductor, Appl. Surf. Sci. 113/114, 291 (1997)

50. S. Kera, H. Setoyama, M. Onoue, K.K. Okudaira, Y. Harada and N. Ueno, Origin of Indium-(3,4,9,10 perylenetetracarboxylic dianhydride) Interface States Studied by Outermost Surface Spectroscopy Using Metastable Atoms, Phys. Rev. B XX, XXX (2000)

51. V.E. Choong, M.G. Mason, C.W. Tang and Y. Gao, Investigation of the Interface Formation Between Calcium and Tris(8-hydroxyquinoline) Aluminum, Appl. Phys. Lett. 72, 2689 (1998)

52. R.Q. Zhang, X.Y. Hou and S.T. Lee, Theory of Magnesium/$Alq_3$ Interaction in Organic Light Emitting Devices, Appl. Phys. Lett. 74, 1612 (1999)

53. N. Johanson, T. Osada, S. Stafström, W.R. Salaneck, V. Parente, D.A. dos Santos, X. Crispin and J.L. Brédas, Electronic Structure of Tris(8-hydroxyquinoline) Aluminum Thin Films in the Pristine and Reduced States, J. Chem. Phys. 111, 2157 (1999)

54. A. Curioni and W. Andreoni, Metal-$Alq_3$ Complexes: the Nature of the Chemical Bonding, J. Am. Chem. Soc. 121, 8216 (1999)

55. P. He, F.C.K. Au, Y.M. Wang, L.F. Cheng, C.S. Lee and S.T. Lee, Direct Evidence for Interaction of Magnesium with Tris(8-hydroxyquinoline) Aluminum, Appl. Phys. Lett. 76, 1422 (2000)

56. B. Bogdanovic, Magnesium Anthracene Systems and Their Application in Synthesis and Catalysis, Acc. Chem. Res., 21, 261 (1988)

57. W. E. Lindsell, Magnesium, Calcium, Strontium and Barium, in *Comprehensive Organometallic Chemistry II,* E. W. Abel, F. G. A. Stone, G. Wilkinson, eds., Oxford, Elsevier, Volume 1, Section 3.3 (1995)

58. G. Parthasarathy, P.E. Burrows, V. Khalfin, V.G. Kozlov and S.R. Forrest, A Metal-Free Cathode for Organic Semiconductor Devices, Appl. Phys. Lett. 72, 2138 (1998)

59. V. Bulović, The Role of Excitons and Interfaces in Molecular Organic Devices, Ph.D. Thesis, Princeton University, 1998 (unpublished)

60. I.G. Hill and A. Kahn, Combined Photoemission / In-Vacuo Transport Study of the ITO/CuPc/α-NPD Molecular Organic Semiconductor System, J. Appl. Phys. 86, 2116 (1999)

61. I.G. Hill, D. Milliron, J. Schwarz and A. Kahn, Organic Semiconductor Interfaces: Electronic Structure and Transport Properties, Appl. Surf. Sci. 166, 354 (2000)

62. I.G. Hill and A. Kahn, Organic Semiconductor Heterointerfaces Containing Bathocuproine, J. Appl. Phys. 86, 4515 (1999)

63. I. Hill and A. Kahn, Energy Level Alignment at Interfaces of Organic Semiconductor Heterostructures, J. Appl. Phys. 84, 5583 (1998)

64. H. Ishii, K. Sugyama, D. Yoshimura, E. Ito, Y. Ouchi and K. Seki, Energy Level Alignment at Model Interfaces of Organic Electroluminescent Devices Studied by UV Photoemission: Trend in the Deviation from the Traditional Way of Estimating the Interfacial Electronic Structures, IEEE J. Sel. Top.Quantum Electron. 4, 24 (1998)

65. M. Pfeiffer, A. Beyer, T. Fritz and K. Leo, Controlled Doping of Phthalocyanine Layers by Cosublimation with Acceptor Molecules: a Systematic Seebeck and Conductivity study, Appl. Phys. Lett. 73, 3202 (1998)

66. A. Nollau, M. Pfeiffer, T. Fritz and K. Leo, Controlled N-Type Doping of a Molecular Organic Semiconductor: Naphthalenetetracarboxylic Dianhydride (NTCDA) Doped with Bis(ethylenedithio)-Tetrathiafulvalene (BEDT-TTF), J. Appl. Phys. 87, 4340 (2000)

67. R. Schlaf, B.A. Parkinson, P.A. Lee, K.W. Nebesny and N.R. Armstrong, HOMO/LUMO Alignment at PTCDA/ZnPc and PTCDA/ClInPc Heterointerfaces Determined by Combined UPS and XPS Measurements, J. Phys. Chem. B 103, 2984 (1999)

68. S.T. Lee, Y.M. Wang, X.Y. Hou and C.W. Tang, Interfacial Electronic Structures in an Organic Light-Emitting Diode, Appl. Phys. Lett. 74, 670 (1999)

69. E.W. Forsythe, V.E. Choong, T.Q. Lee and Y. Gao, Interface Analysis of Naphthyl-Substituted Benzidine Derivative and Tris(8-hydroxyquinoline) Aluminum Using Ultraviolet and X-Ray Photoemission Spectroscopy, J. Vac. Sci. Technol. A 17, 3429 (1999)

70. R. Schlaf, B.A. Parkinson, P.A. Lee, K.W. Nebesny and N.R. Armstrong, Determination of Frontier Orbital Alignment and Band Bending at an Organic Semiconductor Heterointerface by Combined X-Ray and Ultraviolet Photoemission Measurements, Appl. Phys. Lett. 73, 1026 (1998)

71. T. Chassé, C-I Wu, I.G. Hill, and A. Kahn, Band Alignment at Organic-Inorganic Semiconductor Interfaces: α-NPD and CuPc on InP(110), J. Appl. Phys. 85, 6589 (1999)

72. J.-L. Brédas and R. Silbey in Conjugated Polymers, (Kluwer, Dordrecht, 1991)

73. N. Sato, K. Seki, and H. Inokuchi, Polarization Energies of Organic Solids Determined by Ultra-Violet Photoemission Spectroscopy, J. Chem Soc., Faraday Trans. 2, **77**, 1621 (1981)

74. Primary Photoexcitations in Conjugated Polymers: Molecular Exciton versus Semiconductor Band Model, N. S. Sariciftci edit., World Scientific Publishing Co., 1997

75. M. Knupfer, J. Fink, E. Zojer, G. Leising and D. Fichou, Universal Exciton Scaling in π-Conjugated Systems, Chem. Phys. Lett. 318, 585 (2000)

76. Z.G. Zoos, M.H. Hennessy and D. Mukhopadhyay, in Primary photoexcitations in conjugated polymers: molecular exciton versus semiconductor band model, N. S. Sariciftci edit., World Scientific Publishing Co., p. 1 (1997)

77. J.H. Weaver, Electronic-Structures of $C_{60}$, $C_{70}$ and the Fullerides - Photoemission and Inverse Photoemission Studies, J. Phys. Chem. Solids 53, 1433 (1992)

78. J.H. Weaver and D.M. Poirier, Solid State Properties of Fullerenes and Fullerene-based Materials, in Solid State Physics Series 48, H. Ehrenreich and F. Spaepen edits., Academic Press (New York, 1994)

79. G. Gerstenblum, J.J. Pireaux, P.A. Thiry, R. Caudano, J.P. Vigneron, Ph. Lambin, A.A. Lucas and W. Krätschmer, High Resolution Electron Energy Loss Spectroscopy of Thin Films of $C_{60}$on Si(100), Phys. Rev. Lett. 67, 2171 (1991)

80. R.W. Lof, M.A. van Veenendal, B. Koopmans, H.T. Jonkman and G.A. Sawatzky, Band Gap, Exciton, and Coulomb Interaction in Solid $C_{60}$, Phys. Rev. Lett. 68, 3924 (1992)

81. See, for example, R.G. Kepler, J.M. Zeigler, L.A. Harrah and S.R. Kurtz, Photocarrier Generation and Transport in σ-Bonded Polysilanes, Phys. Rev. B 35, 2818 (1987)

82. I.H. Campbell and D.L. Smith, Schottky Energy Barriers and Charge Injection in Metal/$Alq_3$/Metal Structures, Appl. Phys. Lett. 74, 561 (1999)

83. C.B. Duke, W.R. Salaneck, T.J. Fabish, J.J. Ritsko, H.R. Thomas, and A. Paton, Electronic Structure of Pendant-Group Polymers: Molecular-Ion States and Dielectric Properties of Poly(2-vinyl pyridine), Phys. Rev. B 18, 5717 (1978)

84. J.D. Anderson, E.M. McDonald, P.A. Lee, M.L. Anderson, E.L. Ritchie, H.K. Hall, T. Hopkins, E.A. Mash, J. Wang, A. Padias, S. Thayumanavan, S. Barlow, S.R. Marder, G.E. Jabbour. S. Shaheen, B. Kippelen, N. Peyghambarian, R.M. Wightman and N.R. Armstrong , Electrochemistry and Electrogenerated Chemiluminescence Processes of the Components of Aluminum Quinolate/Triarylamine, and Related Organic Light-Emitting Diodes, J. Am. Chem. Soc. 120, 9646(1998)

85. D.K. Slattery, C.A. Linkous and N. Gruhn, Photocatalytic Water-Splitting Using Organic Pigments as Semiconductors, Polymer Preprints 41, 866 (2000)

86. J. Berkowitz, Photoelectron Spectroscopy of Phthalocyanine Vapors, J. Chem Phys. 70, 2819 (1979)

87. W.R. Salaneck, Intermolecular relaxation energies in anthracene, Phys. Rev. Lett. 40, 60 (1978)

88. I.H. Campbell and D.L. Smith, Metal/Organic Energy Barriers: Measurements and Device Implications, (this book)

89. G. Weiser, Stark Effect of One-Dimensional Wannier Excitons in Polydiacetylene Single Crystals, Phys. Rev. B 45, 14076 (1992)

**Table Caption**

The bulk transport gap, $E_t$, is obtained by correction of the UPS-IPES gap, as explained in Ref. [23]; $E_{opt}$ is the absorption peak energy; the charge separation, or exciton binding, energy is $E_t$-$E_{opt}$.

.

| Organic Material | **$E_t$ ±0.4 (eV)** | $E_{opt}$ (eV) | **$E_t$ - $E_{opt}$ ±0.4 (eV)** |
|---|---|---|---|
| CuPc | **2.3** | 1.7 | **0.6** |
| PTCDA | **3.2** | 2.6 | **0.6** |
| α-6T | **3.4** | 3.0 | **0.4** |
| α-NPD | **4.5** | 3.5 | **1.0** |
| $Alq_3$ | **4.6** | 3.2 | **1.4** |

**Figure Captions**

1. Schematic energy diagram of a heterojunction OLED under bias. Electrons (holes) are injected from a low (high) work function cathode (anode) into the electron (hole) transport layer. The heterojunction is designed here to favor exciton formation and radiative recombination in the electron transport layer.

2. Chemical structures of molecules investigated: **$Alq_3$** (tris(8-hydroxy-quinoline)aluminum); **α-NPD** (N,N'-diphenyl-N,N'-bis(l-naphthyl)-l,l'biphenyl-4,4''diamine; **CuPc** (Copper phthalocyanine); **$F_{16}$CuPc** (hexadecafluoro Copper phthalocyanine); **PTCDA** (3,4,9,10 perylenetetracarboxylic dianhydride); **PTCBI** (3,4,9,10 perylenetetracarboxylic bisbenzimidazole); **CBP** (4,4'-N,N'-dicarbazolyl-biphenyl); **BCP** (bathocuproine); and **α-6T** (alpha sexithiophene)

3. He I spectrum of pristine PTCBI showing the valence states with the HOMO and the photoemission cutoff. The Fermi level $E_F$ is measured separately on a Au electrode (from [20] with permission). Inset: chemical structure of the PTCBI molecule.

4. Schematic energy diagram of a metal-organic semiconductor interface (a) without and (b) with a dipole barrier Δ. $\phi_{Be}$ and $\phi_{Bh}$ are the electron and hole barriers, and $E_{vac}(O)$ and $E_{vac}(M)$ are the organic and metal vacuum levels, respectively.

5. Soft X-ray photoemission spectra recorded as a function of deposition of α-NPD on Au. (a) valence states, showing the position of the leading edge of the HOMO with respect to the Au Fermi level; (b) abrupt shift of the photoemission onset indicating the presence of an interface dipole; (c) schematic interface energy diagram deduced from the photoemission measurements.

6. (a) Position of $E_F$ vs. HOMO (and LUMO) as a function of metal work function for six different molecular materials. The data points are obtained via PES for organic-on-metal interfaces. The dashed lines correspond to the Schottky-Mott limit and the vertical lines give the magnitude of the measured interface dipole barriers; (b) Sign and dependence of dipoles vs. metal work function.

7. (a) He I spectra of interfaces formed by incremental deposition of PTCBI on Ag. (b) Top of the valence density of states at the PTCBI/Ag interface. Vertical lines are intended as guides to the eye (from [20] with permission).

8. (a) UPS spectra as a function of $Alq_3$ deposition on Mg. The vertical bar indicates the position of interface gap states (from [45] with permission); (b) Formation of a dipole induced by charge exchanged between the organometallic complex molecules (gap state) and the metal.

9. Soft X-ray photoemission spectra as a function of In deposition on PTCDA: (a) In(4d) core level showing the oxidized state on In; (b) C(1s) core level showing the loss of the carbonyl C peak (B); (c) HOMO and gap region, showing the In-induced gap states (from [48] with permission). The pristine PTCDA molecule and the molecule with In attached to the end groups are represented.

10. Combined UPS/IPES spectra of PTCDA as a function of In deposition. Particularly notable are: the position of $E_F$ near the LUMO on pristine PTCDA; the appearance of gap states upon In deposition; the concomitant decrease in LUMO signal

11. Mg(2p), C(1s), N(1s), O(1s) and Al(2p) core levels measured as a function of Mg deposition on $Alq_3$ (from [45] with permission)

12. Structural representation of the organometallic complex resulting from Mg-$Alq_3$ reaction (from [46] with permission)

13. UPS valence spectra measured as a function of increasing Mg coverage on $Alq_3$ and illustration of corresponding Mg induced shift of molecular levels, or "band bending", at the surface of $Alq_3$

14. (a) Mg/$Alq_3$/Mg structure; Forward (electrons injected from top electrode) and reverse (electrons injected from bottom electrode) current-voltage characteristics of a (b) Mg:Ag/$Alq_3$/Mg:Ag device grown in $10^{-5}$-$10^{-6}$ Torr (from [59] with permission) (c) Mg/$Alq_3$/Mg device; (d) Al/$Alq_3$/Al device; (e) Mg:Ag/ $Alq_3$/Mg:Ag device. The latter three were grown in $10^{-9}$ Torr. (from [45] with permission)

15. (a) Comparison between current-voltage characteristics of ITO/α-NPD and ITO/CuPc/α-NPD devices showing the interlayer-induced increase in hole injection; (b) molecular level alignment diagram constructed using HOMO offsets measured via ultra-violet photoemission spectroscopy (from [60] with permission)

16. He I (21.22 eV) UPS spectra showing the evolution of the top of the valence spectra for the interface formed by depositing α-NPD on CuPc (from [61] with permission)

17. Alignment of molecular levels at organic/organic heterointerfaces (from [61] with permission)

18. Energy level diagram of the α-NPD/InP(110), CuPc/InP(110) and PTCDA/GaAs(100) interfaces. VBM and CBM denote the valence band maximum and conduction band minimum in the inorganic semiconductor.

19. (a) Schematic representation of gas phase and condensed phase PES and IPES, yielding positively charged and negatively charged molecular ions, and polarization of neighboring molecules in the condensed phase. Photon absorption and formation of a Frenkel exciton is also represented; (b) Schematic energy diagram showing (left) the adiabatic ionization energy and electron affinity of the gas phase molecule, (center) relaxed polaron levels, including polarizations $P_+$ and $P_-$, of the molecule in the condensed phase, (right) the optical gap for the neutral excited molecule (from [23] with permission)

20. (a) Comparison between UPS and IPES spectra measured from α-NPD thin film (top) and INDO-simulated UPS and IPES spectra (bottom). The energy scale is referenced to the Fermi level. A compression factor of 1.3 is used to simulate the UPS spectrum and the FWHM is set to 0.5 eV prior to compression. The vertical bars at the bottom of the graph refer to the calculated energies of the molecular

orbitals; (b) LCAO patterns of the HOMO and LUMO levels, calculated at the INDO level α-NPD (from [21] with permission)

21. Composite UPS/IPES spectrum of the filled and empty states recorded from a 50-100Å film of (a) CuPc, (b) PTCDA, (c) α-NPD, and (d) $Alq_3$ deposited on Au. Energy scales are aligned by measuring the Fermi level with UPS and IPES on Au prior to the deposition of the organic film (from [23] with permission)

22. Energy diagram and electron injection barrier at the Mg:Ag/$Alq_3$ interface using (a) the optical gap $E_{opt}$ and (b) the transport gap $E_t$ (gap between the HOMO and LUMO centroids, as defined in the text)

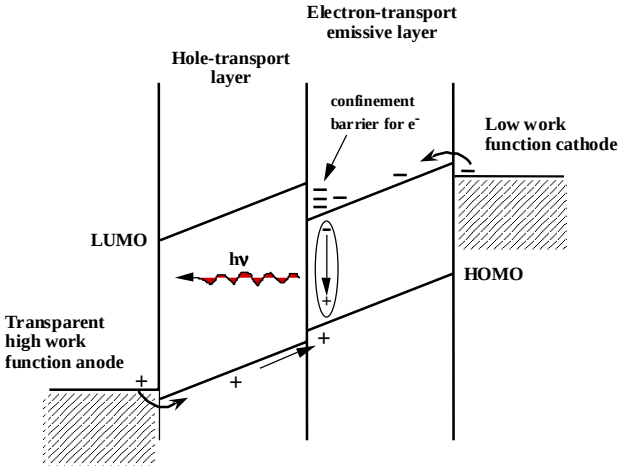


Figure 1

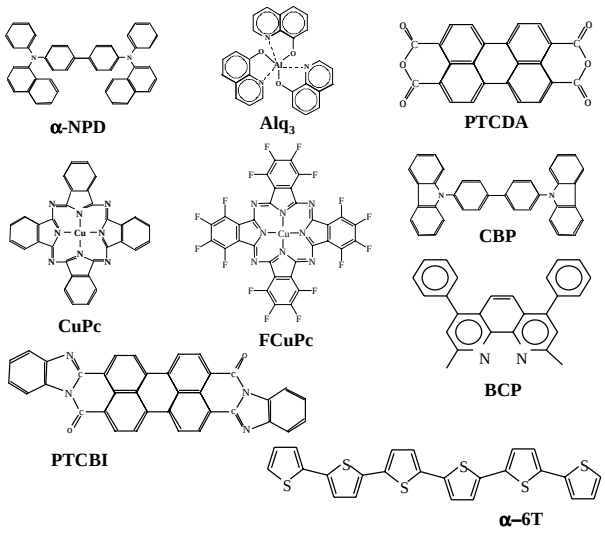


Figure 2

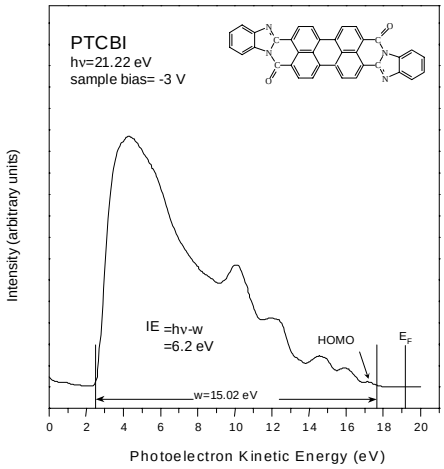


Figure 3

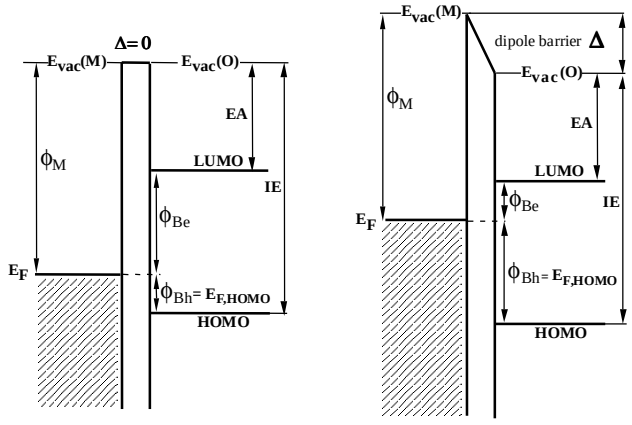


**"Schottky-Mott-like" interface** **Interface dipole**

Figure 4

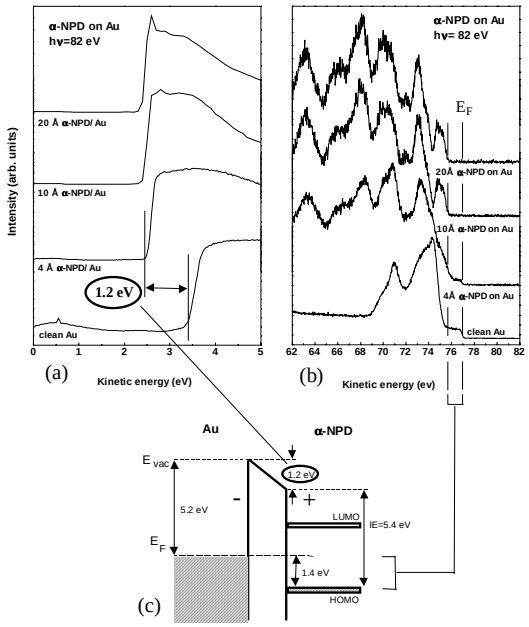


Figure 5

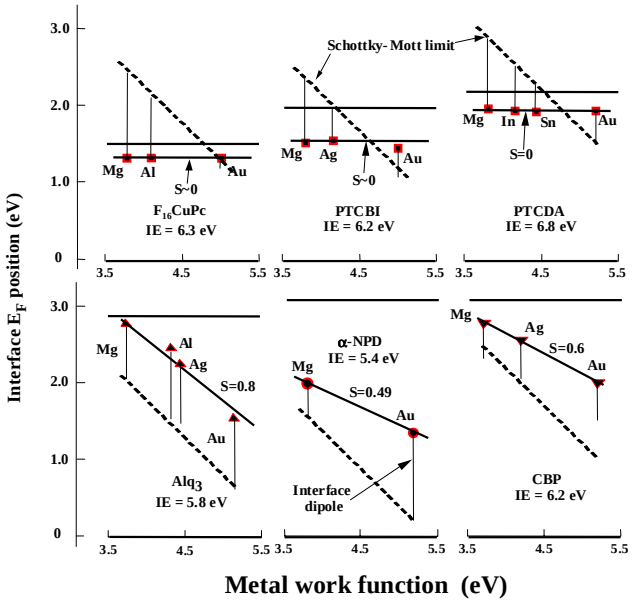


Figure 6a

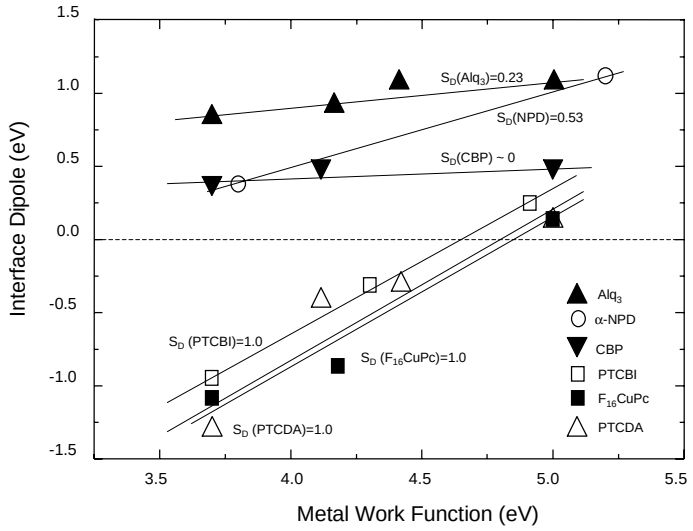


Figure 6b

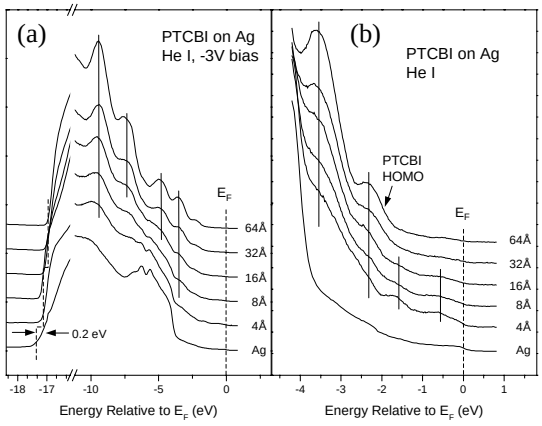


Figure 7

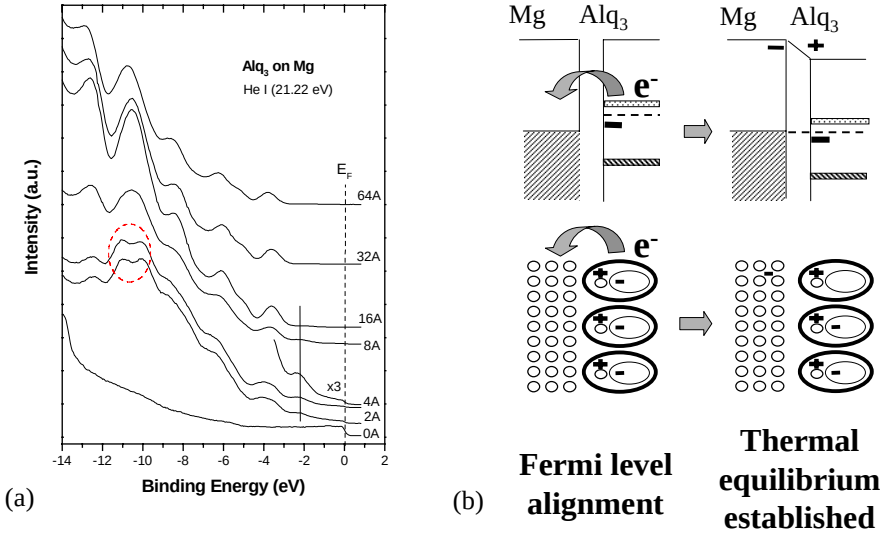


Figure 8

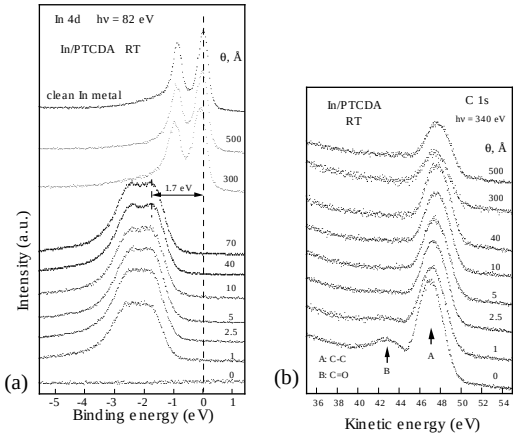


Figure 9

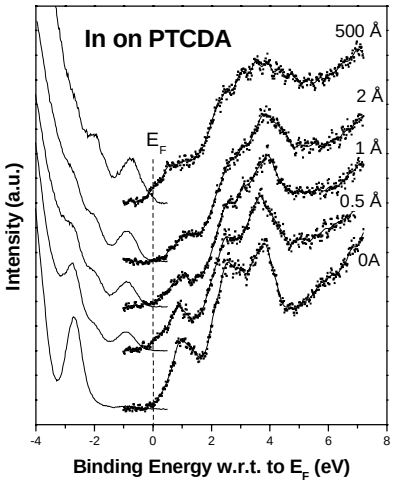


Figure 10

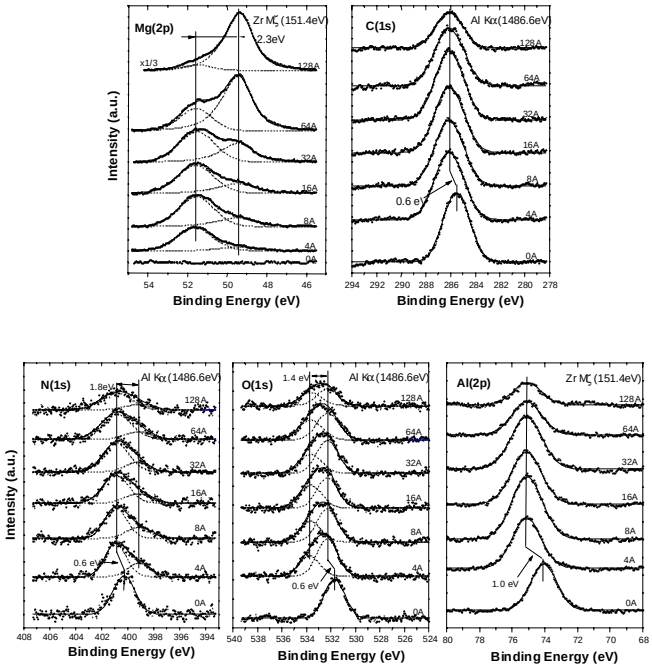


Figure 11

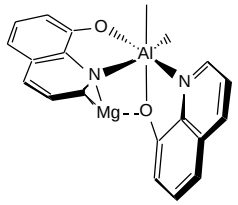


Figure 12

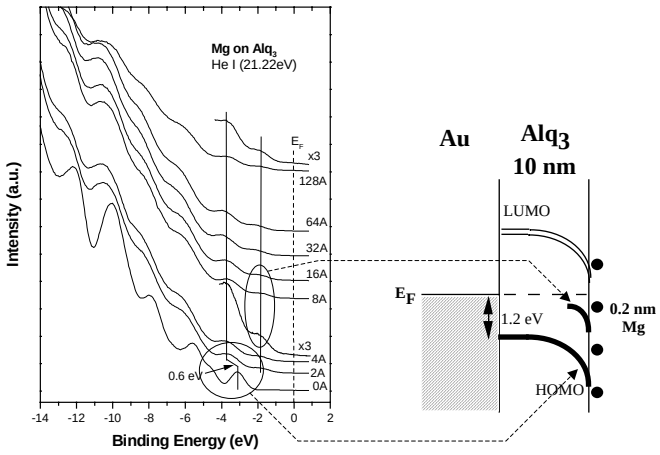


Figure 13

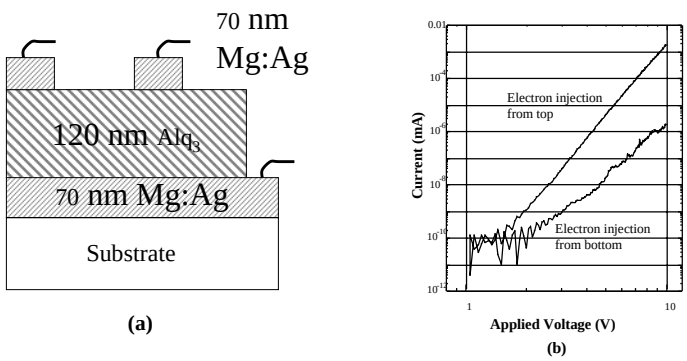


Figure 14

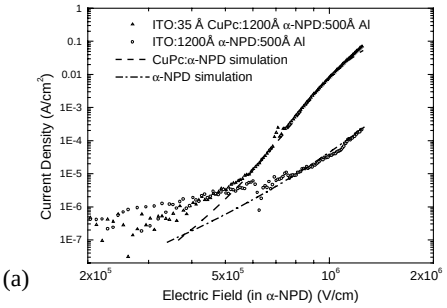


(a)

Figure 15

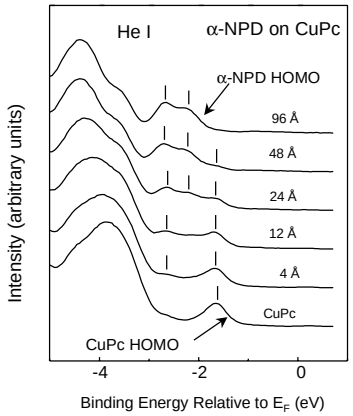


Figure 16

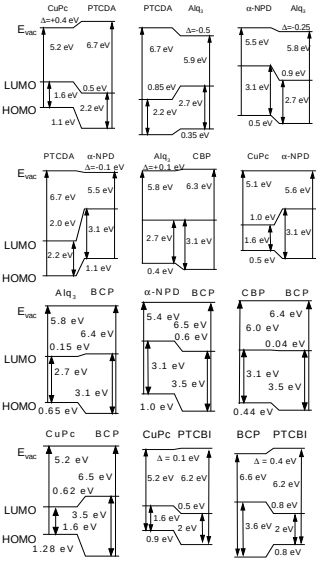


Figure 17

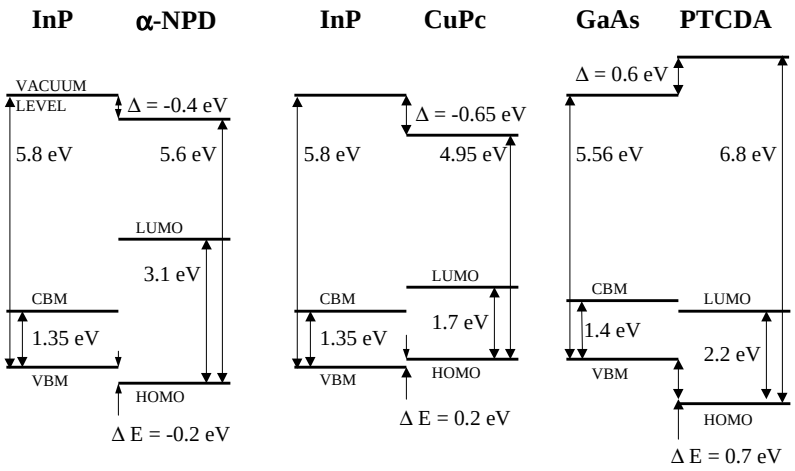


Figure 18

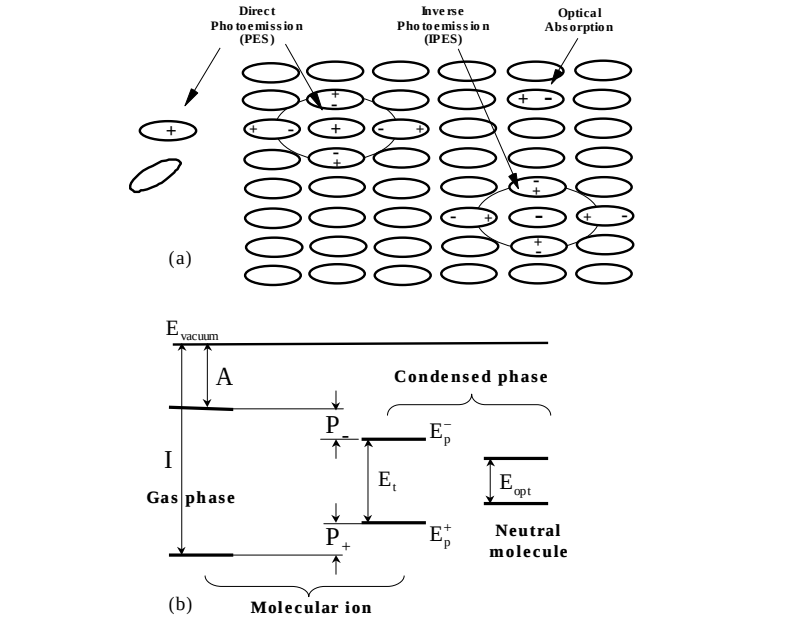


Figure 19

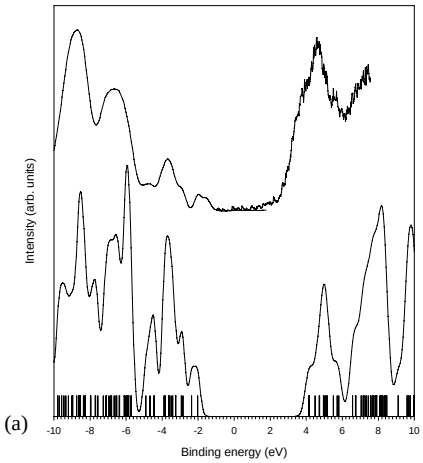


(a)

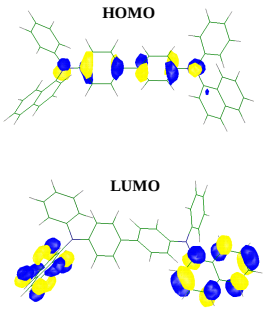


(b)

Figure 20

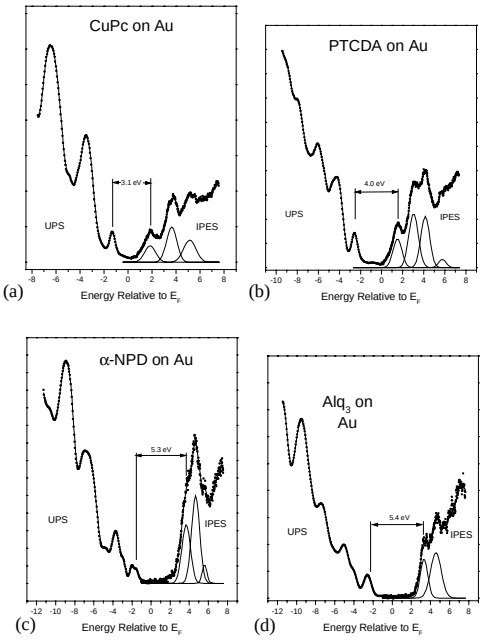


(a) (b) (c) (d)

Figure 21

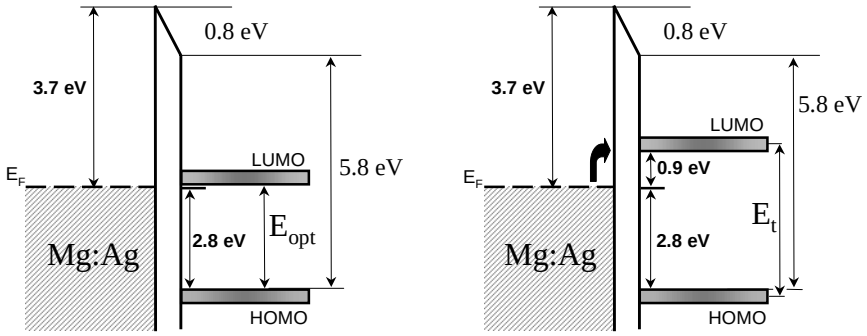
0.8 eV
3.7 eV
LUMO
5.8 eV
$E_F$
2.8 eV
$E_{opt}$
Mg:Ag
HOMO
0.8 eV
3.7 eV
5.8 eV
LUMO
0.9 eV
$E_F$
$E_t$
2.8 eV
Mg:Ag
HOMO

Figure 22